UC San Diego
UC San Diego Previously Published Works

Title
Computational Prediction of the Binding Pose of Metal-Binding Pharmacophores

Permalink
https://escholarship.org/uc/item/78s0w98r

Journal
ACS Medicinal Chemistry Letters, 13(3)

ISSN
1948-5875

Authors
Karges, Johannes
Stokes, Ryjul W
Cohen, Seth M

Publication Date
2022-03-10

DOI
10.1021/acsmedchemlett.1c00584

Peer reviewed

Computational Prediction of the Binding Pose of Metal-Binding Pharmacophores

Johannes Karges, Ryjul W. Stokes, and Seth M. Cohen*

Cite This: *ACS Med. Chem. Lett.* 2022, 13, 428–435

Read Online

ACCESS | Metrics & More | Article Recommendations | Supporting Information

ABSTRACT: Computational modeling of inhibitors for metalloenzymes in virtual drug development campaigns has proven challenging. To overcome this limitation, a technique for predicting the binding pose of metal-binding pharmacophores (MBPs) is presented. Using a combination of density functional theory (DFT) calculations and docking using a genetic algorithm, inhibitor binding was evaluated in silico and compared with inhibitor–enzyme cocrystal structures. The predicted binding poses were found to be consistent with the cocrystal structures. The computational strategy presented represents a useful tool for predicting metalloenzyme–MBP interactions.
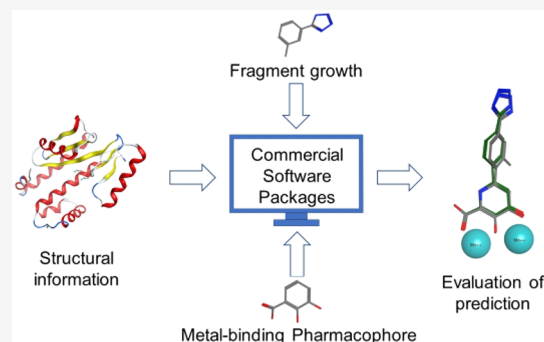
Approximately 40−50% of all enzymes are metal-ion-dependent.[1,2] Typically, the metal ion(s) in these metalloenzymes play either a structural or a catalytic/functional role. For structural purposes, the metal ion ensures proper folding of the protein and allows it to achieve the required three-dimensional shape. Functional metal ions are typically found in the active site where they facilitate catalysis, promote electron transfer, or support substrate binding.[3,4] Despite their diverse biological roles and potential value as drug targets, the development of metalloenzyme inhibitors has lagged. Only ∼7% of FDA-approved drugs in the United States target a metalloenzyme.[5]

Substantial progress has been made to improve the computational algorithms and scoring functions used to find and identify the energetic minimum of an inhibitor–protein complex.[6−9] Despite advancements in computational techniques, predicting accurate binding affinities and geometries of metalloenzyme–inhibitor interactions remains challenging.[10−12] A recent computational study compared the performance of several commonly used docking programs (Auto-Dock4, AutoDock4Zn, AutoDock Vina, Quick Vina 2, LeDock, PLANTS, and UCSF DOCK6) with metalloenzymes. While some of these programs could predict the correct binding geometry of a ligand, none of them were able to successfully rank docking poses.[13] Some attention has also been devoted toward molecular dynamics (MD) strategies. One study demonstrated the docking of inhibitors with a hydroxamic acid metal-binding pharmacophore MBP to Zn^{2+}-dependent matrix metalloproteinase 9 upon dividing the computational process into several tasks: (i) docking with the requirement to generate a metal−MBP interaction of the hydroxamic acid

using the FlexX program, (ii) optimization of the geometry of the MBP−metalloenzyme complex by quantum mechanical and molecular mechanical (QM/MM) calculations, (iii) conformational optimization of the MBP−metalloenzyme complex without changes in the metal−MBP interaction by MD calculations, and (iv) a single-point QM/MM energy calculation. Using this complex workflow, the authors were able to correlate the calculated and experimentally determined binding affinity.[14] However, the aforementioned methods are complex and require significant computational resources and expertise, making them unsuitable for routine virtual screening, docking, and modeling. More user-friendly and accessible methods for predicting metalloenzyme−inhibitor/MBP interactions are needed.

Herein, a readily accessible method for the prediction of MBP−metalloenzyme interactions is presented. The binding pose of the MBP fragment was predicted using a combination of DFT calculations and a genetic algorithm with GOLD. The resulting MBP pose was then extended with Molecular Operating Environment (MOE) and energetically minimized. The method was evaluated against several structurally characterized metalloenzymes from the Protein Data Bank (PDB) with different metal ion active sites and a variety of
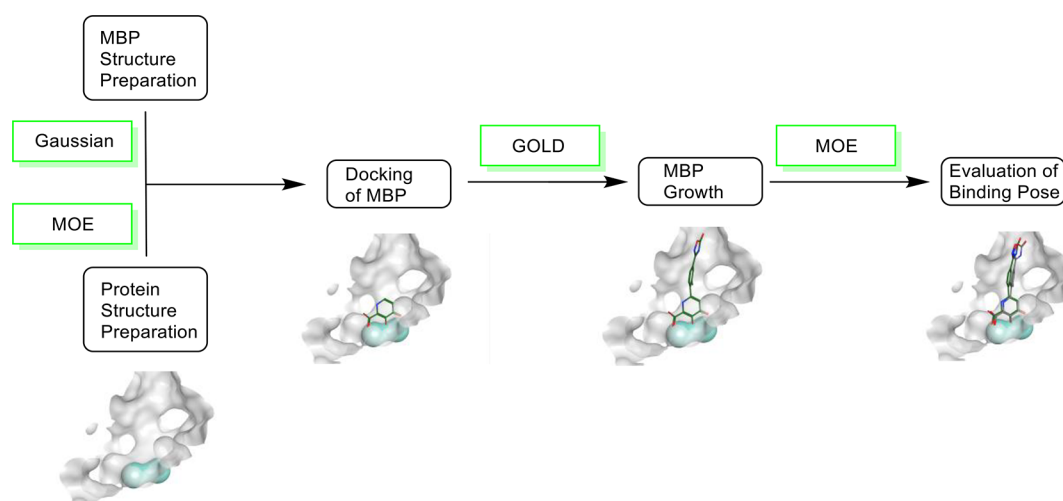
Figure 1. Workflow for modeling metalloenzyme−inhibitor interactions. Protein surface (PA_N) shown in gray, active site metals shown in cyan, and MBPs and inhibitors shown as sticks colored by atom type.

bound inhibitors. The predicted binding poses were found to be in good agreement with the crystallographically determined structures, providing an accessible tool for computational drug discovery campaigns against metalloenzymes.

To ensure the generality of the approach, metalloenzymes were examined that contain different metal ions, different numbers of metal ions in the active site, and varying coordination geometries. The following enzymes were selected

(1) Human carbonic anhydrase II (hCAII): Human carbonic anhydrase II is a Zn^{2+}-dependent metalloenzyme. The active site consists of a tetrahedral Zn^{2+} ion, bound by three His residues and a capping water molecule. The enzyme catalyzes the hydration of carbon dioxide to a bicarbonate anion that modulates carbon dioxide levels, as well as the pH in the bloodstream. hCAII inhibitors are used as a treatment for glaucoma.[15−17]

(2) Jumonji-domain of histone lysine demethylase (KDM): Histone lysine demethylases with a conserved Jumonji-domain are Fe^{2+}-dependent enzymes (crystal structures often possess Ni^{2+} or Mn^{2+} ions as a surrogate for Fe^{2+}). The enzyme active site consists of an octahedral Fe^{2+} ion bound by two His residues and one Glu residue and three capping water molecules. The enzyme catalyzes the demethylation of lysine residues using α-ketoglutaric acid and oxygen. Certain KDMs have been associated with cancer as well as various mental disorders.[18−20]

(3) N-terminal domain of the polymerase acidic subunit of the RNA-dependent RNA polymerase of the influenza virus (PA_N): The N-terminal domain of the polymerase acidic subunit is a Mn^{2+}- or Mg^{2+}-dependent metalloenzyme. The enzyme active site consists of two Mn^{2+} or Mg^{2+} ions, bound by one His, one Ile, one Asp, and two Glu residues and five capping water molecules. The enzyme cleaves a 5′-mRNA cap, which is necessary for eukaryotic translation. PA_N is considered an important pharmacological target against the influenza virus with one compound approved for human use.[21−23]

The modeling experiment was divided into several tasks for which different docking programs were used based on their individual strengths (Figure 1). The three-dimensional structure of an MBP fragment was generated and energetically optimized using density functional theory (DFT) calculations with Gaussian. Other molecule editors (i.e., ORCA, Spartan) were also found to be suitable to generate an appropriate, three-dimensional structure of the MBP. Next, the metalloenzyme−inhibitor structure was obtained from the PDB. Using the MOE software suite, water molecules and other small molecules (e.g., buffer components, cryoprotectant, inhibitors, counterions) were removed, hydrogen atoms were added, and side chains protonated at physiological pH.

The optimized MBP fragments were docked with a genetic algorithm using Genetic Optimization for Ligand Docking (GOLD). The structure of the protein was considered rigid, and the metal ions in the active site were set with a predefined coordination geometry (e.g., tetrahedral, octahedral). The resulting binding poses were evaluated during docking using the ChemPLP scoring function. Following this, the binding poses from the docking experiment were rescored using the GoldScore scoring function. Previous studies have shown that rescoring improves the identification of fragment hits compared to use of a single scoring function.[24,25] Because docking with GOLD requires high computational resources that would limit virtual screening of large libraries, the docking process was divided into two tasks. The MBP was docked using GOLD, followed by virtual MBP "fragment growth" into a lead-like molecule using MOE. To elaborate the MBP fragment into the complete inhibitor, the MBP model obtained from GOLD was loaded into MOE, and the MBP was manually elaborated to generate the complete inhibitor. The inhibitor was then energetically minimized, while the pose of the MBP generated by GOLD was kept fixed.

To ensure that the metalloenzyme structures studied here are highly homologous, the amino acid sequences and three-dimensional structures were compared. As expected, each target was found with a sequence homology of at least ~93% and a sequence coverage of at least ~91% (Table S1). Notably, portions of the structures that did not align were the termini, which were not resolved in all structures. To evaluate the accuracy of the inhibitor docking, the computational and crystallographic structures were aligned using MOE using a protein alignment algorithm. The sequences of the structures were aligned, and then, the three-dimensional structures were superimposed. While the aligned proteins showed generally a
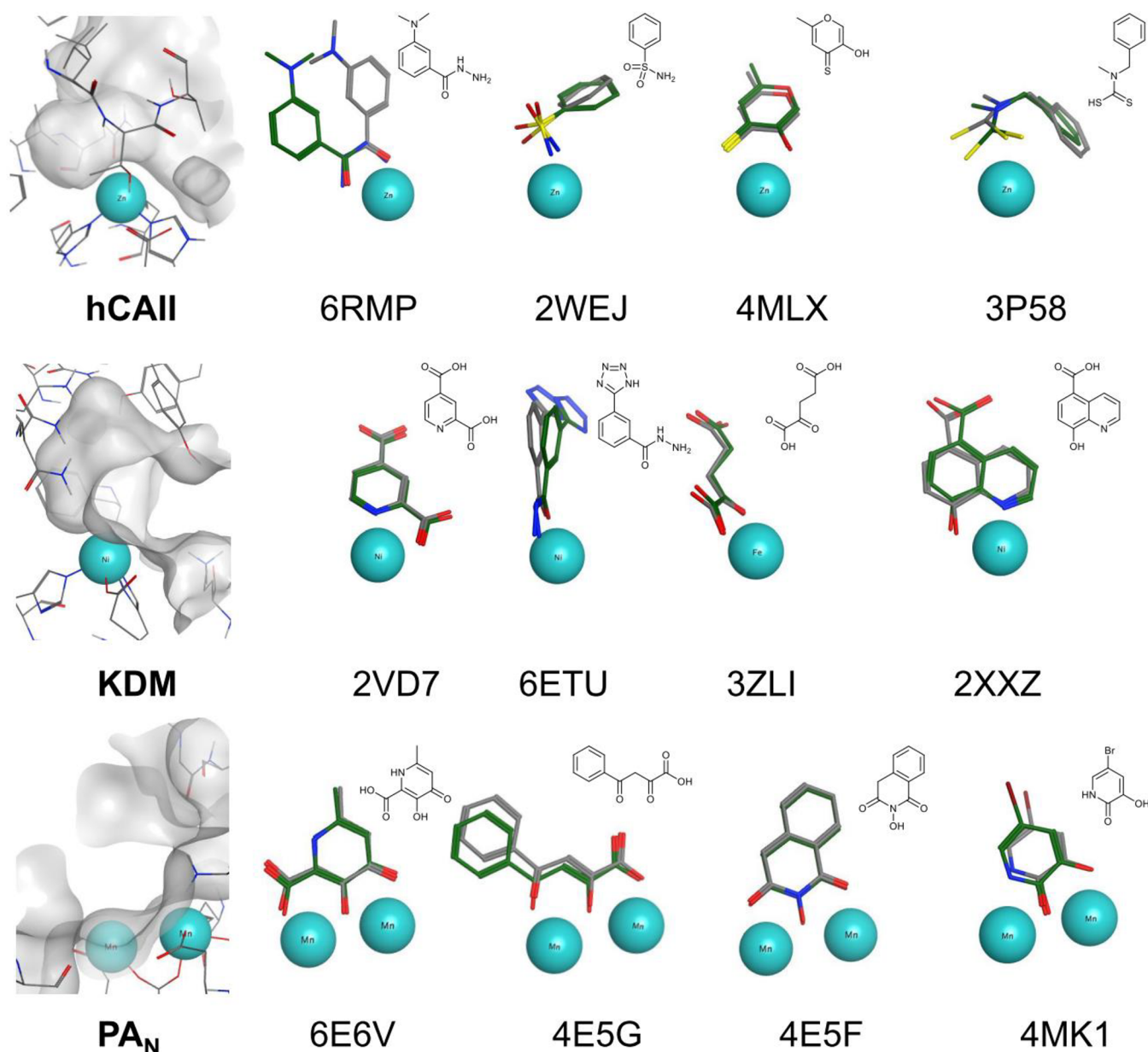
Figure 2. Comparison of MBP binding poses from crystallographic determined structures (gray carbons, PDB entry codes shown) to computational docking (green carbons) using GOLD.

Table 1. RMSD Values of Computationally and Crystallographically Determined Metalloenzyme−MBP Complexes

enzyme	entry	RMSD/Å	reference
hCAII	2WEJ	0.49	27
	3P58	0.86	28
	4MLX	0.32	29
	6RMP	3.75	30
KDM	2VD7	0.22	31
	2XXZ	0.68	32
	3ZLI	0.34	33
	6ETU	0.94	34
PA$_N$	4E5F	0.23	35
	4E5G	0.63	35
	4MK1	1.67	36
	6E6V	0.34	37

high congruency, some portions of the structures showed significant discrepancies. To improve the superposition, the structures were further aligned with a focus on the active site, specifically on the metal ion(s) and adjacent amino acid atoms as a reference point (see Supporting Information for details). As a means to quantify the difference between the computational and crystallographic binding geometries, the root-mean-square deviation (RMSD) values were calculated using LigRMSD 1.0.[26]

To validate the docking methodology, four structurally diverse and crystallographically characterized MBPs for each metalloenzyme target were examined.[27−37] Using DFT calculations and docking with GOLD, the best scoring binding poses of all MBPs with hCAII and PA$_N$ and the majority of MBPs with KDM were found coordinated to the active site metal ion(s). In the case of 2,4-pyridinedicarboxylic acid with KDM (PDB 2VD7), the MBP did not dock to the active site
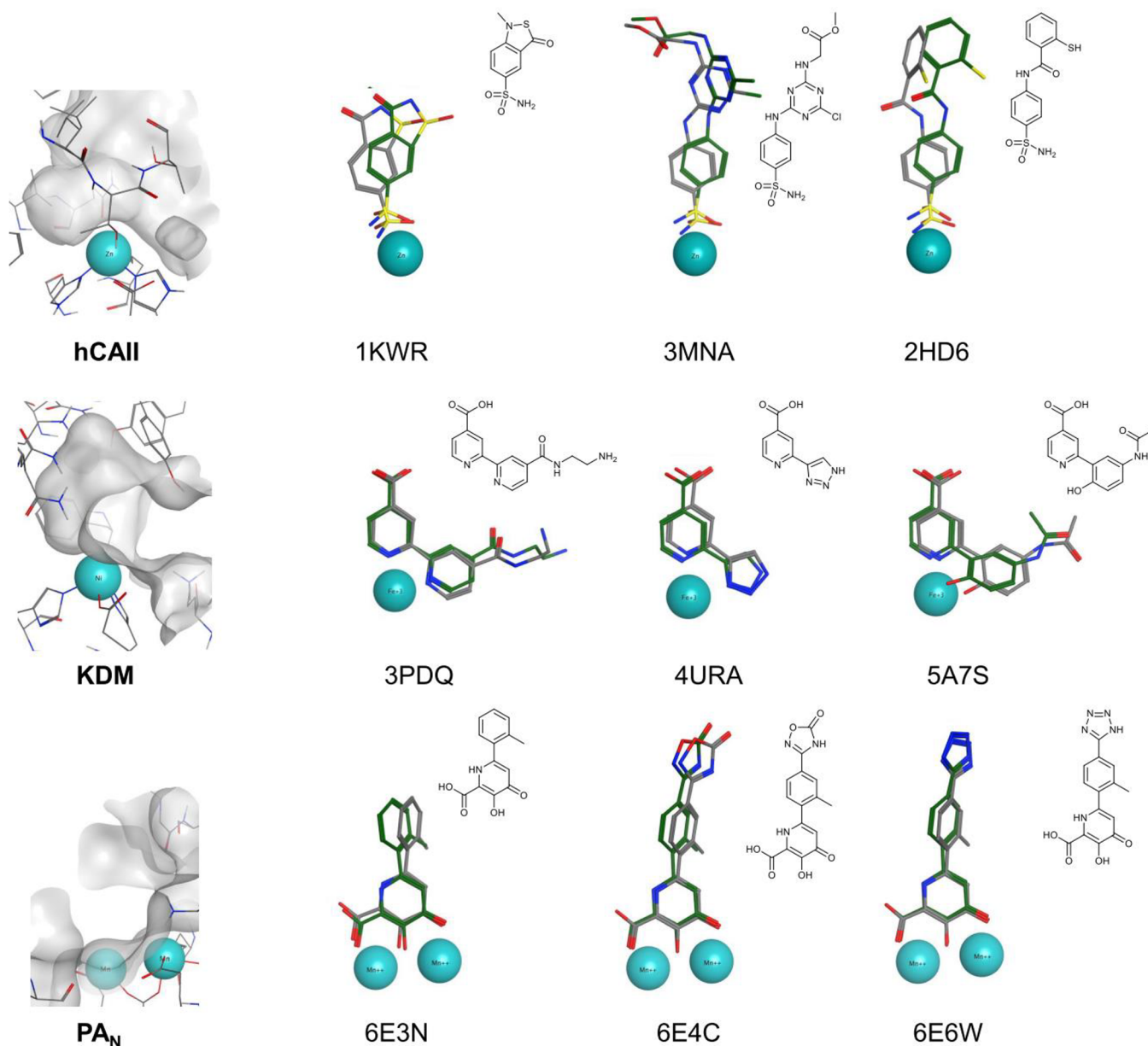
Figure 3. Comparison of binding modes of crystallographically determined structures (gray carbons, PDB entry codes shown) to computationally derived inhibitor poses (green carbons).

but rather at a distal site (Figure S1). To address this outlier, docking was repeated with a box of 20 Å centered around the KDM active site resulting in 2,4-pyridinedicarboxylic acid docked to the active site metal ion in KDM.

The computational binding poses were compared to the crystallographic structures. A visual comparison shows good alignment for the vast majority of the modeled and experimentally determined metalloenzyme−MBP complexes (Figure 2). The only fragment that showed a significant discrepancy was 3-(dimethylamino)benzohydrazide (PDB 6RMP) bound to hCAII. This MBP was computationally predicted to bind the metal with the keto hydrazide moiety in an orientation that was reversed from the crystallographic structure. The quality of the docking was quantified by determining the RMSD values between the computational and crystallographic configurations. As expected, the predicted

binding poses of the MBP fragment were found to be in good agreement with an average RMSD value of 0.87 Å (Table 1).

Following successful MBP geometry prediction, the modeling of lead-like inhibitors based on these MBPs was performed. A total of 47 crystal structures of metalloenzyme−inhibitor complexes from the PDB were examined. Specifically, benzenesulfonamide inhibitors with hCAII,[38−55] 4-pyridine-carboxylic acid inhibitors with KDM,[31,56−63] and 3-hydroxy-4-oxo-1,4-dihydropyridine-2-carboxylic acid inhibitors with PA$_N$[35,37,64] were modeled. The bound inhibitors were selected to have broad chemical composition to test the generality of the methodology (Figures S2−S4). To verify the binding pose of the MBP fragment, the computational poses from GOLD were compared to the crystal structures of bound lead-like inhibitors, comparing only the MBP moiety (Figure S5). Overall, the fragments showed good agreement to the experimental binding geometries with RMSD values of 0.90
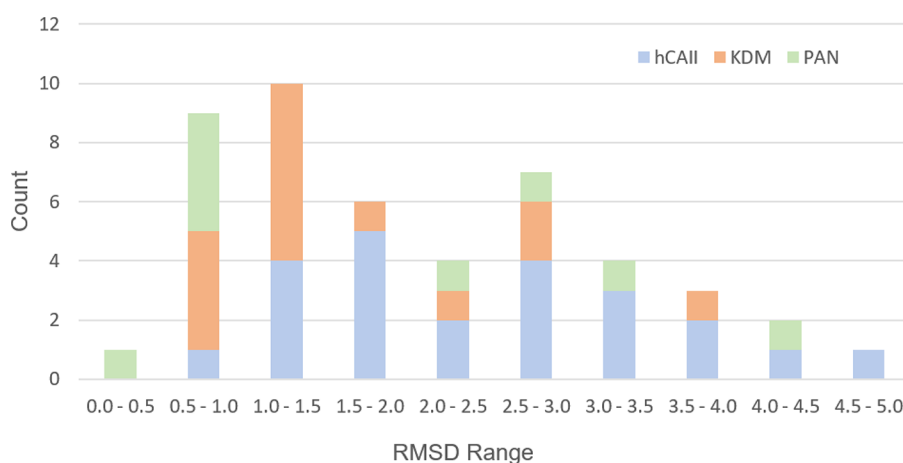
Figure 4. Distribution of RMSD values of computational and experimental binding poses for metalloenzyme inhibitors. Color-coded by metalloenzyme: hCAII (blue), KDM (orange), and PA$_N$ (green).

Å for hCAII, 0.52 Å for KDM, and 0.78 Å for PA$_N$ (for a complete list of RMSD values, see Table S2). That stated, while the crystallographically characterized binding poses for the fragments bound to hCAII and KDM were very similar, the MBPs for PA$_N$ were found in more varied orientations across the crystal structures (Figure S5C,D). While the bond distances for MBPs in PA$_N$ were all similar, the MBPs are bound with orientational differences relative to the active site. A binding angle was arbitrarily defined between the carbon atom of the carboxyl group of Asp108, a centroid between both metal centers, and a centroid of the aromatic MBP moiety. This angle ranged from 175° (PDB 4E5I, Figure S5) to 145° (PDB 6E3N, Figure S5) across structures and likely originates from the influence of other interactions that the full-length inhibitors form with subpockets in the relatively large, open active site of PA$_N$.

The benzenesulfonamide fragment in hCAII showed the largest RMSD discrepancy between the docked and experimental structures. These differences could negatively influence the next stage in the docking the full-length inhibitor, where ligand extension of the predicted binding pose for the MBP could lead to inaccuracies in the full ligand pose. Therefore, a modified MBP docking protocol was used for the benzenesulfonamide fragment in hCAII. The binding pose of the MBP is primarily driven by metal coordination and hydrogen bonding interactions of the sulfonamide moiety with hCAII. Therefore, the docking of this fragment was repeated with a weighting bias that added additional metal-binding terms to the GoldScore scoring function, as previously described.[65] With these adjustments to the scoring function, the binding pose of benzenesulfonamide was better aligned with the experimentally determined structures (Figure S6) and produced a low RMSD value of 0.47 Å (Table S3). This experiment shows that additional information about expected MBP−active site interactions can be used to better predict the binding pose. To avoid adding a user bias in applying our method (caused by modifying the applied scoring function), the initial binding pose (Figure S5) was used for the further ligand extensions.

As described above, the three-dimensional protein structures of the computationally and experimentally determined enzyme−inhibitor complexes were superimposed using an automatic algorithm and then further refined with focus on the active site with an intentional bias toward the active site metal

ion(s) as well as the coordinating amino acids (Figure S7). As the inhibitors are expected to coordinate to the metal ion as part of their mechanism of action, these elements should be aligned with the highest possible accuracy. This procedure resulted in average RMSD values of 0.23 Å for hCAII, 0.13 Å for KDM, and 0.14 Å for PA$_N$ for the respective active site alignments.

Following the protein structure alignment, the computationally and experimentally determined enzyme−inhibitor complexes were compared (Figures 3 and S8−S10). Overall, a high congruency between the docked models and the experimentally determined binding poses is observed with average RMSD values of 2.44 Å for hCAII, 1.57 Å for KDM, and 1.60 Å for PA$_N$ (for a full list of RMSD values, see Table S4). Noteworthily, the discrepancies of the computationally modeled and experimentally determined binding poses are within the average resolution of the crystal structure within the PDB, with most entries having a resolution of 1.8−2.0 Å.[66]

The RMSD distribution of the structure alignments was analyzed (Figure 4). While a few of the docked compounds showed large discrepancies to the experimentally determined structures (RMSD >4 Å), the majority of docked inhibitors were in good agreement with the experimental structures, with RMSD values well within the resolution range of typical protein−inhibitor cocrystal structures (RMSD <2 Å). These results suggest that the computational approach described here could be useful for the developing MBP fragments into lead-like compounds via fragment growth.

Finally, the docking method was compared with commonly used docking programs AutoDock Vina (Figure S11) and SwissDock (Figure S12) under standard docking procedures using hCAII and PA$_N$ as model systems. Upon applying these methods, MBPs were not found in the active sites, and the results were not consistent with the crystallographically characterized structures. These findings further highlight the value of the methods described here for the prediction of binding poses of inhibitors in metalloenzymes.

A new computational strategy for modeling the binding of MBPs in metalloenzymes is presented. The approach uses a combination of DFT calculations and docking with a genetic algorithm (GOLD). The method was evaluated by comparing computational models with experimentally determined metalloenzyme−inhibitor complexes. Metalloenzymes with different metal ions, different numbers of metal ions in the active site,

and different metal coordination geometries were examined to determine the scope and robustness of the approach. Good agreement was found between the computational models and experimentally determined structures, well within the resolution of most crystal structures in the PDB. The workflow described here is a robust method for predicting MBP binding poses, and further computational methods that address energetic optimization of complete, lead-like inhibitors would be useful next steps in improved modeling of metalloenzyme inhibitors. Overall, the presented methodology may provide a more accessible approach for the design of novel metalloenzyme inhibitors.

■ ASSOCIATED CONTENT

Ⓢ Supporting Information

The Supporting Information is available free of charge at https://pubs.acs.org/doi/10.1021/acsmedchemlett.1c00584.

> Structure preparation, protein sequence homology, fragment docking, protein alignment, fragment growth, evaluation of binding pose prediction, percent sequence identity and percent sequence coverage table, protein–MBP binding pose, fragment and full-length inhibitor structures, RMSD values of MBPs, overlay of docked and crystallographic MBPs, overlay of docked and crystallographic MBPs with metal-binding bias, RMSD values of docked and crystallographic MBPs with metal-binding bias, active site alignment, comparison of binding modes, comparison with other docking programs, and RMSD values of full-length inhibitors (PDF)

■ AUTHOR INFORMATION

Corresponding Author

Seth M. Cohen − *Department of Chemistry and Biochemistry, University of California, San Diego, La Jolla, California 92093, United States;* ⓘ orcid.org/0000-0002-5233-2280; Email: scohen@ucsd.edu

Authors

Johannes Karges − *Department of Chemistry and Biochemistry, University of California, San Diego, La Jolla, California 92093, United States;* ⓘ orcid.org/0000-0001-5258-0260

Ryjul W. Stokes − *Department of Chemistry and Biochemistry, University of California, San Diego, La Jolla, California 92093, United States*

Complete contact information is available at:
https://pubs.acs.org/10.1021/acsmedchemlett.1c00584

Notes

The authors declare the following competing financial interest(s): S.M.C. is a cofounder of and has an equity interest in Cleave Therapeutics, Forge Therapeutics, and Blacksmith Medicines, companies that may potentially benefit from the research results. S.M.C. also serves on the Scientific Advisory Board for Blacksmith Medicines and serves on the Scientific Advisory Board and receives compensation from Forge Therapeutics. The terms of this arrangement have been reviewed and approved by the University of California, San Diego in accordance with its conflict of interest policies.

■ ABBREVIATIONS

DFT, density functional theory; FDA, Food and Drug Administration; hCAII, human carbonic anhydrase II; KDM, Jumonji-domain of histone lysine demethylase; MBP, metal-binding pharmacophore; MD, molecular dynamics; MM, molecular mechanical; PA_N, N-terminal domain of the polymerase acidic subunit of the RNA-dependent RNA polymerase of the influenza virus; PDB, Protein Data Bank; QM, quantum mechanical; RMSD, root-mean-square deviation

■ REFERENCES

(1) Andreini, C.; Bertini, I.; Cavallaro, G.; Holliday, G. L.; Thornton, J. M. Metal Ions In Biological Catalysis: From Enzyme Databases To General Principles. *J. Biol. Inorg. Chem.* **2008**, *13*, 1205−1218.

(2) Waldron, K. J.; Rutherford, J. C.; Ford, D.; Robinson, N. J. Metalloproteins And Metal Sensing. *Nature* **2009**, *460*, 823−830.

(3) Yang, Y.; Hu, X.-Q.; Li, Q.-S.; Zhang, X.-X.; Ruan, B.-F.; Xu, J.; Liao, C. Metalloprotein Inhibitors for the Treatment of Human Diseases. *Curr. Top. Med. Chem.* **2016**, *16*, 384−396.

(4) Nastri, F.; D'Alonzo, D.; Leone, L.; Zambrano, G.; Pavone, V.; Lombardi, A. Engineering Metalloprotein Functions In Designed And Native Scaffolds. *Trends Biochem. Sci.* **2019**, *44*, 1022−1040.

(5) Chen, A. Y.; Adamek, R. N.; Dick, B. L.; Credille, C. V.; Morrison, C. N.; Cohen, S. M. Targeting Metalloenzymes For Therapeutic Intervention. *Chem. Rev.* **2019**, *119*, 1323−1455.

(6) Pagadala, N. S.; Syed, K.; Tuszynski, J. Software For Molecular Docking: A Review. *Biophys. Rev.* **2017**, *9*, 91−102.

(7) Sulimov, V. B.; Kutov, D. C.; Sulimov, A. V. Advances In Docking. *Curr. Med.* **2020**, *26*, 7555−7580.

(8) Morris, G. M.; Lim-Wilby, M. Molecular Docking. *Molecular Modeling of Proteins* **2008**, *443*, 365−382.

(9) Kitchen, D. B.; Decornez, H.; Furr, J. R.; Bajorath, J. Docking And Scoring In Virtual Screening For Drug Discovery: Methods And Applications. *Nat. Rev. Drug Discovery* **2004**, *3*, 935−949.

(10) Sciortino, G.; Rodríguez-Guerra Pedregal, J.; Lledós, A.; Garribba, E.; Maréchal, J.-D. Prediction Of The Interaction Of Metallic Moieties With Proteins: An Update For Protein-Ligand Docking Techniques. *J. Comput. Chem.* **2018**, *39*, 42−51.

(11) Chen, E.; Swift, R. V.; Alderson, N.; Feher, V. A.; Feng, G.-S.; Amaro, R. E. Computation-Guided Discovery Of Influenza Endonuclease Inhibitors. *ACS Med. Chem. Lett.* **2014**, *5*, 61−64.

(12) Englebienne, P.; Fiaux, H.; Kuntz, D. A.; Corbeil, C. R.; Gerber-Lemaire, S.; Rose, D. R.; Moitessier, N. Evaluation Of Docking Programs For Predicting Binding Of Golgi α-Mannosidase II Inhibitors: A Comparison With Crystallography. *Proteins* **2007**, *69*, 160−176.

(13) Çınaroğlu, S. S.; Timuçin, E. Comparative Assessment Of Seven Docking Programs On A Nonredundant Metalloprotein Subset Of The PDBbind Refined. *J. Chem. Inf. Model.* **2019**, *59*, 3846−3859.

(14) Khandelwal, A.; Lukacova, V.; Comez, D.; Kroll, D. M.; Raha, S.; Balaz, S. A Combination Of Docking, QM/MM Methods, And MD Simulation For Binding Affinity Estimation Of Metalloprotein Ligands. *J. Med. Chem.* **2005**, *48*, 5437−5447.

(15) Eriksson, A. E.; Jones, T. A.; Liljas, A. Refined Structure Of Human Carbonic Anhydrase II At 2.0 Å Resolution. *Proteins* **1988**, *4*, 274−282.

(16) De Simone, G.; Alterio, V.; Supuran, C. T. Exploiting The Hydrophobic And Hydrophilic Binding Sites For Designing Carbonic Anhydrase Inhibitors. *Expert Opin. Drug Discovery* **2013**, *8*, 793−810.

(17) McKenna, R.; Supuran, C. T. Carbonic Anhydrase Inhibitors Drug Design. *Carbonic Anhydrase: Mechanism, Regulation, Links to Disease, and Industrial Applications* **2014**, *75*, 291−323.

(18) Fueyo, R.; García, M. A.; Martínez-Balbás, M. A. Jumonji Family Histone Demethylases In Neural Development. *Cell Tissue Res.* **2015**, *359*, 87−98.

(19) Shi, Y. Histone Lysine Demethylases: Emerging Roles In Development, Physiology And Disease. *Nat. Rev. Genet.* **2007**, *8*, 829−833.

(20) Pedersen, M. T.; Helin, K. Histone Demethylases In Development And Disease. *Trends Cell Biol.* **2010**, *20*, 662−671.

(21) Reich, S.; Guilligay, D.; Pflug, A.; Malet, H.; Berger, I.; Crépin, T.; Hart, D.; Lunardi, T.; Nanao, M.; Ruigrok, R. W. H.; Cusack, S. Structural Insight Into Cap-Snatching And RNA Synthesis By Influenza Polymerase. *Nature* **2014**, *516*, 361−366.

(22) Ju, H.; Zhang, J.; Huang, B.; Kang, D.; Huang, B.; Liu, X.; Zhan, P. Inhibitors Of Influenza Virus Polymerase Acidic (PA) Endonuclease: Contemporary Developments And Perspectives. *J. Med. Chem.* **2017**, *60*, 3533−3551.

(23) Karges, J.; Stokes, R. W.; Cohen, S. M. Photorelease Of A Metal-Binding Pharmacophore From A Ru(ii) Polypyridine Complex. *Dalton Trans.* **2021**, *50*, 2757−2765.

(24) Oda, A.; Tsuchida, K.; Takakura, T.; Yamaotsu, N.; Hirono, S. Comparison of Consensus Scoring Strategies for Evaluating Computational Models of Protein−Ligand Complexes. *J. Chem. Inf. Model.* **2006**, *46*, 380−391.

(25) Cheng, T.; Li, X.; Li, Y.; Liu, Z.; Wang, R. Comparative Assessment of Scoring Functions on a Diverse Test Set. *J. Chem. Inf. Model.* **2009**, *49*, 1079−1093.

(26) Velázquez-Libera, J. L.; Durán-Verdugo, F.; Valdés-Jiménez, A.; Núñez-Vivanco, G.; Caballero, J. LigRMSD: A Web Server For Automatic Structure Matching And RMSD Calculations Among Identical And Similar Compounds In Protein-Ligand Docking. *Bioinformatics* **2020**, *36*, 2912−2914.

(27) Scott, A. D.; Phillips, C.; Alex, A.; Flocco, M.; Bent, A.; Randall, A.; O'Brien, R.; Damian, L.; Jones, L. H. Thermodynamic Optimisation In Drug Discovery: A Case Study Using Carbonic Anhydrase Inhibitors. *ChemMedChem.* **2009**, *4*, 1985−1989.

(28) Carta, F.; Aggarwal, M.; Maresca, A.; Scozzafava, A.; McKenna, R.; Supuran, C. T. Dithiocarbamates: A New Class Of Carbonic Anhydrase Inhibitors. Crystallographic And kinetic Investigations. *Chem. Commun.* **2012**, *48*, 1868−1870.

(29) Martin, D. P.; Blachly, P. G.; Marts, A. R.; Woodruff, T. M.; de Oliveira, C. A. F.; McCammon, J. A.; Tierney, D. L.; Cohen, S. M. 'Unconventional' Coordination Chemistry By Metal Chelating Fragments In A Metalloprotein Active Site. *J. Am. Chem. Soc.* **2014**, *136*, 5400−5406.

(30) Glöckner, S.; Heine, A.; Klebe, G. A Proof-of-Concept Fragment Screening Of A Hit-Validated 96-Compounds Library Against Human Carbonic Anhydrase II. *Biomolecules* **2020**, *10*, 518.

(31) Rose, N. R.; Ng, S. S.; Mecinović, J.; Liénard, B. M. R.; Bello, S. H.; Sun, Z.; McDonough, M. A.; Oppermann, U.; Schofield, C. J. Inhibitor Scaffolds For 2-Oxoglutarate-Dependent Histone Lysine Demethylases. *J. Med. Chem.* **2008**, *51*, 7053−7056.

(32) Che, K. H.; Yue, W. W.; Krojer, T.; Muniz, J. R. C.; Ng, S. S.; Tumber, A.; Daniel, M.; Burgess-Brown, N.; Savitsky, P.; Ugochukwu, E.; Filippakopoulos, P.; Arrowsmith, C.; Weigelt, J.; Edwards, A.; Bountra, C.; Oppermann, U. Crystal structure of the human JMJD3 jumonji domain, PDB 2XXZ. *Protein Data Bank*, 2010.

(33) Walport, L. J.; Hopkinson, R. J.; Vollmar, M.; Madden, S. K.; Gileadi, C.; Oppermann, U.; Schofield, C. J.; Johansson, C. Human UTY(KDM6C) Is A Male-Specific N^ϵ-Methyl Lysyl Demethylase. *J. Biol. Chem.* **2014**, *289*, 18302−18313.

(34) Małecki, P. H.; Rüger, N.; Roatsch, M.; Krylova, O.; Link, A.; Jung, M.; Heinemann, U.; Weiss, M. S. Structure-Based Screening Of Tetrazolylhydrazide Inhibitors Versus KDM4 Histone Demethylases. *ChemMedChem.* **2019**, *14*, 1828−1839.

(35) DuBois, R. M.; Slavish, P. J.; Baughman, B. M.; Yun, M.-K.; Bao, J.; Webby, R. J.; Webb, T. R.; White, S. W. Structural And Biochemical Basis For Development Of Influenza Virus Inhibitors Targeting The PA Endonuclease. *PLoS Pathog.* **2012**, *8*, e1002830.

(36) Bauman, J. D.; Patel, D.; Baker, S. F.; Vijayan, R. S. K.; Xiang, A.; Parhi, A. K.; Martínez-Sobrido, L.; LaVoie, E. J.; Das, K.; Arnold, E. Crystallographic Fragment Screening And Structure-Based Optimization Yields A New Class Of Influenza Endonuclease Inhibitors. *ACS Chem. Bio.* **2013**, *8*, 2501−2508.

(37) Credille, C. V.; Morrison, C. N.; Stokes, R. W.; Dick, B. L.; Feng, Y.; Sun, J.; Chen, Y.; Cohen, S. M. SAR Exploration Of Tight-Binding Inhibitors Of Influenza Virus PA Endonuclease. *J. Med. Chem.* **2019**, *62*, 9438−9449.

(38) Kim, C.-Y.; Chandra, P. P.; Jain, A.; Christianson, D. W. Fluoroaromatic−Fluoroaromatic Interactions Between Inhibitors Bound In The Crystal Lattice Of Human Carbonic Anhydrase II. *J. Am. Chem. Soc.* **2001**, *123*, 9620−9627.

(39) Grzybowski, B. A.; Ishchenko, A. V.; Kim, C.-Y.; Topalov, G.; Chapman, R.; Christianson, D. W.; Whitesides, G. M.; Shakhnovich, E. I. Combinatorial Computational Method Gives New Picomolar Ligands For A Known Enzyme. *Proc. Natl. Acad. Sci. U. S. A.* **2002**, *99*, 1270−1273.

(40) Grüneberg, S.; Stubbs, M. T.; Klebe, G. Successful Virtual Screening For Novel Inhibitors Of Human Carbonic Anhydrase: Strategy And Experimental Confirmation. *J. Med. Chem.* **2002**, *45*, 3588−3602.

(41) De Simone, G.; Vitale, R. M.; Di Fiore, A.; Pedone, C.; Scozzafava, A.; Montero, J.-L.; Winum, J.-Y.; Supuran, C. T. Carbonic Anhydrase Inhibitors: Hypoxia-Activatable Sulfonamides Incorporating Disulfide Bonds That Target the Tumor-Associated Isoform IX. *J. Med. Chem.* **2006**, *49*, 5544−5551.

(42) Behnke, C. A.; Le Trong, I.; Godden, J. W.; Merritt, E. A.; Teller, D. C.; Bajorath, J.; Stenkamp, R. E. Atomic Resolution Studies Of Carbonic Anhydrase II. *Acta Crystallogr. D* **2010**, *66*, 616−627.

(43) Carta, F.; Garaj, V.; Maresca, A.; Wagner, J.; Avvaru, B. S.; Robbins, A. H.; Scozzafava, A.; McKenna, R.; Supuran, C. T. Sulfonamides Incorporating 1,3,5-Triazine Moieties Selectively And Potently Inhibit Carbonic Anhydrase Transmembrane Isoforms IX, XII And XIV Over Cytosolic Isoforms I And II: Solution And X-ray Crystallographic Studies. *Bioorg. Med. Chem.* **2011**, *19*, 3105−3119.

(44) Pacchiano, F.; Aggarwal, M.; Avvaru, B. S.; Robbins, A. H.; Scozzafava, A.; McKenna, R.; Supuran, C. T. Selective Hydrophobic Pocket Binding Observed Within The Carbonic Anhydrase II Active Site Accommodate Different 4-Substituted-Ureido-Benzenesulfonamides And Correlate To Inhibitor Potency. *Chem. Commun.* **2010**, *46*, 8371−8373.

(45) Biswas, S.; Carta, F.; Scozzafava, A.; McKenna, R.; Supuran, C. T. Structural Effect Of Phenyl Ring Compared To Thiadiazole Based Adamantyl-Sulfonamides On Carbonic Anhydrase Inhibition. *Bioorg. Med. Chem.* **2013**, *21*, 2314−2318.

(46) Güzel-Akdemir, Ö.; Biswas, S.; Lastra, K.; McKenna, R.; Supuran, C. T. Structural Study Of The Location Of The Phenyl Tail Of Benzene Sulfonamides And The Effect On Human Carbonic Anhydrase Inhibition. *Bioorg. Med. Chem.* **2013**, *21*, 6674−6680.

(47) Buratto, J.; Colombo, C.; Stupfel, M.; Dawson, S. J.; Dolain, C.; Langlois d'Estaintot, B.; Fischer, L.; Granier, T.; Laguerre, M.; Gallois, B.; Huc, I. Structure Of A Complex Formed By A Protein And A Helical Aromatic Oligoamide Foldamer At 2.1 Å Resolution. *Angew. Chem., Int. Ed.* **2014**, *53*, 883−887.

(48) Alterio, V.; Tanc, M.; Ivanova, J.; Zalubovskis, R.; Vozny, I.; Monti, S. M.; Di Fiore, A.; De Simone, G.; Supuran, C. T. X-ray Crystallographic And Kinetic Investigations Of 6-Sulfamoyl-Saccharin As A Carbonic Anhydrase Inhibitor. *Org. Biomol. Chem.* **2015**, *13*, 4064−4069.

(49) Runtsch, L. S.; Barber, D. M.; Mayer, P.; Groll, M.; Trauner, D.; Broichhagen, J. Azobenzene-Based Inhibitors Of Human Carbonic Anhydrase II. *Beilstein J. Org. Chem.* **2015**, *11*, 1129−1135.

(50) La Regina, G.; Coluccia, A.; Famiglini, V.; Pelliccia, S.; Monti, L.; Vullo, D.; Nuti, E.; Alterio, V.; De Simone, G.; Monti, S. M.; Pan, P.; Parkkila, S.; Supuran, C. T.; Rossello, A.; Silvestri, R. Discovery Of 1,1′-Biphenyl-4-Sulfonamides As A New Class Of Potent And Selective Carbonic Anhydrase XIV Inhibitors. *J. Med. Chem.* **2015**, *58*, 8564−8572.

(51) Nocentini, A.; Ferraroni, M.; Carta, F.; Ceruso, M.; Gratteri, P.; Lanzi, C.; Masini, E.; Supuran, C. T. Benzenesulfonamides Incorporating Flexible Triazole Moieties Are Highly Effective Carbonic Anhydrase Inhibitors: Synthesis And Kinetic, Crystallographic, Computational, And Intraocular Pressure Lowering Investigations. *J. Med. Chem.* **2016**, *59*, 10692−10704.

(52) Ferraroni, M.; Cornelio, B.; Sapi, J.; Supuran, C. T.; Scozzafava, A. Sulfonamide Carbonic Anhydrase Inhibitors: Zinc Coordination And Tail Effects Influence Inhibitory Efficacy And Selectivity For Different Isoforms. *Inorg. Chim. Acta* **2018**, *470*, 128−132.

(53) Alterio, V.; Esposito, D.; Monti, S. M.; Supuran, C. T.; De Simone, G. Crystal Structure Of The Human Carbonic Anhydrase II Adduct With 1-(4-sulfamoylphenyl-ethyl)-2,4,6-triphenylpyridinium Perchlorate, A Membrane-Impermeant, Isoform Selective Inhibitor. *J. Enzyme Inhib. Med. Chem.* **2018**, *33*, 151−157.

(54) Glöckner, S.; Ngo, K.; Sager, C. P.; Hüfner-Wulsdorf, T.; Heine, A.; Klebe, G. Conformational Changes In Alkyl Chains Determine The Thermodynamic And Kinetic Binding Profiles Of Carbonic Anhydrase Inhibitors. *ACS Chem. Biol.* **2020**, *15*, 675−685.

(55) Nocentini, A.; Alterio, V.; Bua, S.; Micheli, L.; Esposito, D.; Buonanno, M.; Bartolucci, G.; Osman, S. M.; Alothman, Z. A.; Cirilli, R.; Pierini, M.; Monti, S. M.; Di Cesare Mannelli, L.; Gratteri, P.; Ghelardini, C.; De Simone, G.; Supuran, C. T. Phenyl(thio)-phosphon(amid)ate Benzenesulfonamides As Potent And Selective Inhibitors Of Human Carbonic Anhydrases II And VII Counteract Allodynia In A Mouse Model Of Oxaliplatin-Induced Neuropathy. *J. Med. Chem.* **2020**, *63*, 5185−5200.

(56) Chang, K.-H.; King, O. N. F.; Tumber, A.; Woon, E. C. Y.; Heightman, T. D.; McDonough, M. A.; Schofield, C. J.; Rose, N. R. Inhibition Of Histone Demethylases By 4-Carboxy-2,2′-Bipyridyl Compounds. *ChemMedChem.* **2011**, *6*, 759−764.

(57) King, O. N. F.; Krojer, T.; Arrowsmith, C. H.; Edwards, A.; Bountra, C.; McDonough, M. A.; Schofield, C. J. Crystal Structure Of JMJD2A Complexed With Inhibitor, PDB 4GD4. *Protein Data Bank*, 2012.

(58) England, K. S.; Tumber, A.; Krojer, T.; Scozzafava, G.; Ng, S. S.; Daniel, M.; Szykowska, A.; Che, K.; von Delft, F.; Burgess-Brown, N. A.; Kawamura, A.; Schofield, C. J.; Brennan, P. E. Optimisation Of A Triazolopyridine Based Histone Demethylase Inhibitor Yields A Potent And Selective KDM2A (FBXL11) Inhibitor. *Med. Chem. Commun.* **2014**, *5*, 1879−1886.

(59) Korczynska, M.; Le, D. D.; Younger, N.; Gregori-Puigjané, E.; Tumber, A.; Krojer, T.; Velupillai, S.; Gileadi, C.; Nowak, R. P.; Iwasa, E.; Pollock, S. B.; Ortiz Torres, I.; Oppermann, U.; Shoichet, B. K.; Fujimori, D. G. Docking And Linking Of Fragments To Discover Jumonji Histone Demethylase Inhibitors. *J. Med. Chem.* **2016**, *59*, 1580−1598.

(60) Roatsch, M.; Robaa, D.; Pippel, M.; Nettleship, J. E.; Reddivari, Y.; Bird, L. E.; Hoffmann, I.; Franz, H.; Owens, R. J.; Schüle, R.; Flaig, R.; Sippl, W.; Jung, M. Substituted 2-(2-aminopyrimidin-4-yl)-pyridine-4-carboxylates As Potent Inhibitors Of JumonjiC Domain-Containing Histone Demethylases. *Future Med. Chem.* **2016**, *8*, 1553−1571.

(61) Bavetsias, V.; Lanigan, R. M.; Ruda, G. F.; Atrash, B.; McLaughlin, M. G.; Tumber, A.; Mok, N. Y.; Le Bihan, Y.-V.; Dempster, S.; Boxall, K. J.; Jeganathan, F.; Hatch, S. B.; Savitsky, P.; Velupillai, S.; Krojer, T.; England, K. S.; Sejberg, J.; Thai, C.; Donovan, A.; Pal, A.; Scozzafava, G.; Bennett, J. M.; Kawamura, A.; Johansson, C.; Szykowska, A.; Gileadi, C.; Burgess-Brown, N. A.; von Delft, F.; Oppermann, U.; Walters, Z.; Shipley, J.; Raynaud, F. I.; Westaway, S. M.; Prinjha, R. K.; Fedorov, O.; Burke, R.; Schofield, C. J.; Westwood, I. M.; Bountra, C.; Müller, S.; van Montfort, R. L. M.; Brennan, P. E.; Blagg, J. 8-Substituted Pyrido[3,4-d]pyrimidin-4(3H)-one Derivatives As Potent, Cell Permeable, KDM4 (JMJD2) And KDM5 (JARID1) Histone Lysine Demethylase Inhibitors. *J. Med. Chem.* **2016**, *59*, 1388−1409.

(62) Nie, Z.; Shi, L.; Lai, C.; O'Connell, S. M.; Xu, J.; Stansfield, R. K.; Hosfield, D. J.; Veal, J. M.; Stafford, J. A. Structure-Based Design And Discovery Of Potent And Selective KDM5 Inhibitors. *Bioorg. Med. Chem. Lett.* **2018**, *28*, 1490−1494.

(63) Chen, Y. K.; Bonaldi, T.; Cuomo, A.; Del Rosario, J. R.; Hosfield, D. J.; Kanouni, T.; Kao, S.-c.; Lai, C.; Lobo, N. A.; Matuszkiewicz, J.; McGeehan, A.; O'Connell, S. M.; Shi, L.; Stafford, J. A.; Stansfield, R. K.; Veal, J. M.; Weiss, M. S.; Yuen, N. Y.; Wallace, M. B. Design Of KDM4 Inhibitors With Antiproliferative Effects In Cancer Models. *ACS Med. Chem. Lett.* **2017**, *8*, 869−874.

(64) Credille, C. V.; Dick, B. L.; Morrison, C. N.; Stokes, R. W.; Adamek, R. N.; Wu, N. C.; Wilson, I. A.; Cohen, S. M. Structure−Activity Relationships In Metal-Binding Pharmacophores For Influenza Endonuclease. *J. Med. Chem.* **2018**, *61*, 10206−10217.

(65) Kirton, S. B.; Murray, C. W.; Verdonk, M. L.; Taylor, R. D. Prediction Of Binding Modes For Ligands In The Cytochromes P450 And Other Heme-Containing Proteins. *Proteins* **2005**, *58*, 836−844.

(66) Brzezinski, D.; Dauter, Z.; Minor, W.; Jaskolski, M. On The Evolution Of The Quality Of Macromolecular Models In The PDB. *FEBS J.* **2020**, *287*, 2685−2698.